International Journal of Engineering & Technology, 7 (2.23) (2018) 475-478

International Journal of Engineering & Technology

Website: www.sciencepubco.com/index.php/IJET

Research paper

Analysis of Plastic Flow Localization in Bimetal Electrolytically Saturated with Hydrogen

S. Barannikova[1,2,3*], Yu. Li [1], A. Malinovskiy [3], L. Zuev [1]

[1]Strength Physics Laboratory, Institute Of Strength Physics And Materials Science, SB RAS, Tomsk, 634055, Russia
[2]Faculty Of Physics And Engineering, National Research Tomsk State University, Tomsk, 634050, Russia
[3]Faculty Of Civil Engineering, Tomsk State University Of Architecture And Building, Tomsk, 634003, Russia
**Corresponding Author E-Mail: Bsa@Ispms.Tsc.Ru*

Abstract

Plastic deformation of bimetal compound of austenitic stainless and low-carbon construction steels, resistant to corrosion, is localized through the digital image correlation method upon the uniaxial tension of sample. The evolution of zones of plastic deformation in bimetal is inspected upon the onset of the process and is exposed to hydrogen saturation in a three-electrode electrochemical cell at a controlled constant cathode potential for 6 hours. Localized plastic deformation zones are found to form and evolve during the tension of bimetal samples both at the onset and after 6 hour of the electrolytic hydrogenation throughout the plastic yielding in the primary, protective and transitional layers of the bimetal. The bimetal fracture is initiated by stress concentrated in the bimetal transition layer. Nucleation and propagation of a crack is observed at early work-hardening stages. The fracture of bimetal after hydrogenation is established to be more ductile as compared with precursor.

Keywords: *Plastic deformation; Hydrogen; Localization; Bimetal; Fracture.*

1. Introduction

Scientists are continually attempting to discover novel composites with outstanding properties for industrial applications [1]. Recently identified multi-layer composites together with their machining and joining processes are reported in [2]. Bimetals, composed of two metals and alloys (cladding steel), refer to this kind of materials. Unlike conventional steels that are composed of cladding materials, cladding steel not only retains cost, but also provides other outstanding properties, such as high mechanical strength and excellent resistance to heat and corrosion. This enables these materials to be extensively applied in petroleum, chemical, medical, and nuclear industries [3-6].

In this study, bimetal was composed of 301 AISI austenitic stainless steel and A 283 Grade low-carbon steel. Stainless steel exhibits high corrosion resistance and stability in gaseous and aqueous media, but also specific strength superior to that of low carbon steel. Carbon steel possesses satisfactory strength and lesser cost compared to stainless steel, but weaker stability to the environment and corrosion resistance. Recently, the attempts to elaborate mechanically reliable stainless steel/carbon steel bimetal have been to a large extent because of the scarcity of the materials with enhanced corrosion resistance, good environmental stability, increased specific strength and low production cost [7].

Multilayer metals undergo severe plastic deformation during operation. However, a very few works are devoted to elucidation of deformation peculiarities of bimetals. To date, plastic deformation heterogeneities at macro- , meso- and microscopic scales have been identified and examined for a great variety of pure metals and alloys [8, 9]. At the macroscopic level, the plastic deformation exhibits non-uniform localization from yield stress to failure. Various forms of this plastic deformation localization refer to different types of auto waves, depending on a strain hardening law that dominates at this stage. According to early works [10], plastic flows in bimetals are reliably detected through the auto waves approach for the description of localized plastic deformation data in FCC, BCC and HCP of metals and alloys, gathered on an AL-MEC-tv measuring complex for digital recording of speckle images.

The above bimetal composite comprising low carbon steel and austenitic stainless steel is a convenient model material for inspecting localized deformation features after the electrolytic hydrogenation of multi-layered metals combined with BCC- and FCC-lattices. The presence of hydrogen in solid solutions in steels is mainly thanks to a small diameter of this element and to its ability to diffuse easily in solid state. Solubilization and/or diffusion rates of hydrogen in steels are affected by different factors, such as temperature of molding, composition, crystalline structure and substructure of alloy. Meanwhile, the presence of hydrogen in metals and especially in steels is often undesirable, because hydrogen alters to a great extent the mechanical and metallurgic parameters of these materials, even causing their fracture [11-14]. In this connection, the current study is aimed at elucidating the impact of dissolved hydrogen on the macroscopic plastic flow localization patterns in a bimetal composite of austenitic stainless steel and low-carbon steel.

2. Material and Methods

Flat specimens with gauge length dimensions of 42×8×2 mm3 were fabricated from the austenitic stainless steel - low-carbon steel bimetal composite (301 AISI - A 283 Grade C) produced via pouring and rolled to achieve a required thickness of 8 mm. The cladding layer was 0.6-mm-thick. Pouring a liquid metal onto a

solid plate placed in a mold is frequently utilized for producing various bimetals [15].
The electrolytic hydrogenation of bimetal samples was carried out within 6 hours under a controlled cathode potential of -600 mV relative to a reference electrode of silver chloride in 0.1N sulphuric acid solution with addition of 20 mg/L of thiourea [16]. The current-voltage curves were obained on an IPC-Compact potentiostat. The time between hydrogen loading and tensile test was less than 30 min and the testing time did not exceed 60 min.
Previously subjected to the form of dog bones, specimens were stretched at T = 300 K with a rate of 6.67×10-5 s-1 on a LFM-125 testing machine. The patterns of plastic deformation centers during the uniaxial tension have been acquired through the digital image correlation (DIC) technique [17, 18] and the novel approach for visualization of plastic flow localization, underlying the first-order statistics of laser speckle patterns [19]. The local deformation distribution parameters have been evaluated, as well.

3. Results and Discussion

The deformation curves upon the tension of 301 AISI - A 283 Grade C stainless steel bimetal composite specimens are plotted in Fig. 1. The plastic flow curve is associated with the general diagrams described by the Lüdwig equation:

$$\sigma(\varepsilon) = \sigma_y + \theta\varepsilon^n \quad (1)$$

where θ is the deformation hardening coefficient and n is the deformation hardening exponent. The values of n strain exponent vary in different portions of a stress-strain curve and changes in a stepwise manner depending on the degree of strain. Particular constant values of n and θ correspond to each of the plastic deformation stages. The mechanical properties of probed steel in different states are listed in Table 1.

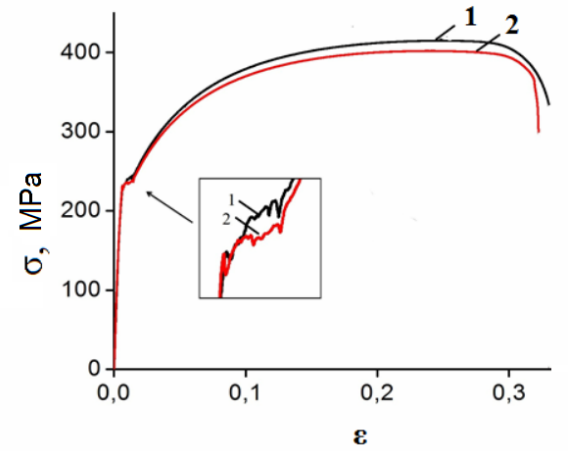

Fig. 1: Stress-strain curves for bimetal in the onset (1) and after 6 h of electrolytic hydrogenation (2).

Table1 1: Mechanical properties of bimetal in different states

Material	σ_y (MPa)	σ_B (MPa)	δ (%)
Onset (1)	241	414	31
6 h hydrogenation (2)	237	400	33

An inspection of the loading curve evidences the emergence of the yield plateau and yield drop (Fig. 1, line 1). The yield plateau extent with a yield drop is 0.008 that is owing to the Lüders band propagation in the precursor's range (A 283 Grade C).
The analysis of steps in the loading diagrams of initial bimetal specimens from the work hardening coefficient $\theta = d\sigma / d\varepsilon$ and the constant value n (here n is the deformation hardening exponent in the Lüdwik equation) reveal the following peculiarities of the deformation curves for a sample. A transition segment from the elastic part to the plastic flow is supervened by the yield plateau that is replaced with a linear-hardening step at the total deformation ε_{tot} = 0.03 ÷ 0.055. The succeeding process is the Taylor parabolic work-hardening with the constant n =1/2 and total deformation of ε_{tot} =0.12 ÷ 0.20, and, finally, there is the pre-fracture stage with n ~ 0.3 and ε_{tot} =0.24 ÷ 0.29.
According to data for a bimetal after 6 h of electrical saturation with hydrogen, a stress-strain curve (Fig. 1, line 2) comprises the linear-hardening stage with the total deformation of ε_{tot} = 0.04 ÷ 0.062. It is followed by the Taylor parabolic work-hardening with n =1/2 and ε_{tot} =0.13 ÷ 0.25, and by the pre-fracture stage with n ~0.3 and ε_{tot} =0.26 ÷ 0.30.
Plastic deformation of a composite is evidenced by from the Lüders band interface in the bimetal (Fig. 2). However, 301 AISI stainless steel of the high-strength cladding metal prevents the Lüders band propagation with a constant velocity from the clamp of the machine, served as a basic stress concentrator. This results in the abrupt movement of the initial band together with the origin and propagation of other Lüders bands through the specimen section from the cladding metal - basic metal interface. The occurrence of stress concentrators is favored by the bending moments that arise during the bimetal's plastic deformation. The propagation of the local elongations on the yield plateau is the relay propagation of the Lüders band fronts which appear near the clamps and at the opposite interfaces. The Lüders fronts are shifted (Fig. 2) and vanish when meeting each other on the yield plateau.

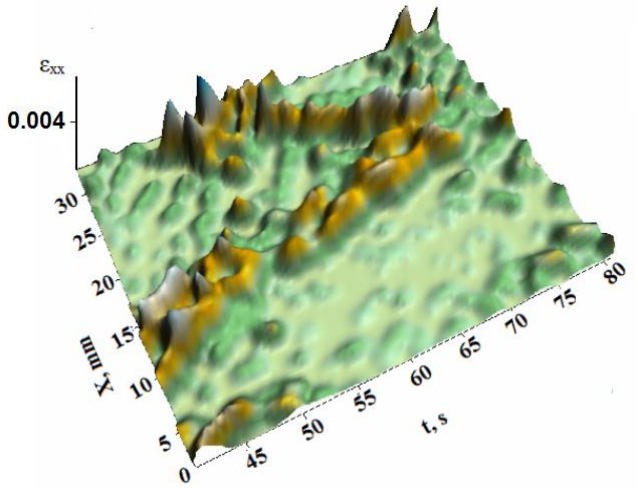

Fig.2: Visualization of the Lüders band propagation through the initial bimetal length.

The propagation rate velocity of zones with localized plastic deformation was found from the kinetic diagrams (Figs. 3a and 3b). For the Lüders band, it was equal 2.4×10-4 m/s, while for the linear work hardening it enriched 6×10-5 m/s.

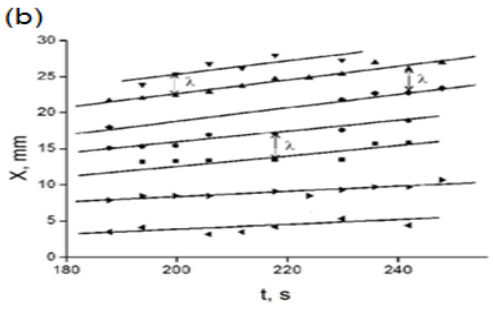

Fig.3: Kinetic plots X(t) for a strain localization zone along the sample's axis on (a) the yield plateau and at (b) the linear deformation hardening.

As is seen from the parabolic, the plastic flow localization can be visualized as a stationary system of plastic flow centers through the specimen length with a distance λ = 4 mm between them (Fig.

4a). At the pre-fracture stage, the immobile zones of plastic strain localization begin moving consistently with a tendency to merge into a high-amplitude focus of localized straining (Fig. 4 b), where a neck-like narrowing of the sample's cross section is observed (Figs. 5a and 5b). This maximum coincides with the occurring damage. The bimetal damage feature is the plastic deformation heterogeneity within the intermediate layer of the metal, where the stress concentrator looking like a trihedral prism is formed at the microlevel (Fig. 5a). The fragmentation of specimen sets the fracture pattern of the bimetal composite. So, a pair of macro bands, related to localized plastic deformation, arises during the shoulder effect over a range of the stress macro concentrator. Both bands propagate along the conjugated directions of the maximum shear stress across the whole section of the sample, forming the trihedral prisms at the macro level on the bond interface of the bimetal. The cracks are nucleated through the parent metal region at the trihedral prism tip and stay then gradually merged, passing across the whole section of the metal sample. The fracture of hydrogenized samples is more ductile as compared with the precursor, meaning that hydrogen atoms increase the plasticity of the austenitic stainless steel layer of the test bimetal (Fig. 5b).

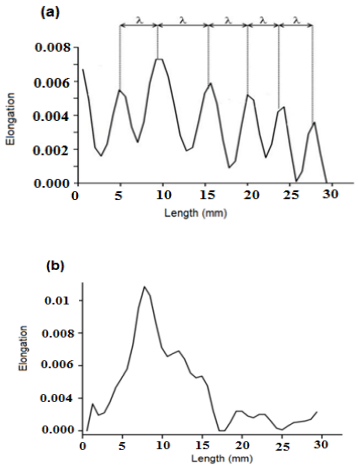

Fig. 4: Local elongation ε_{xx} along the extension axis during (a) parabolic strain hardening and (b) pre-fracture stages.

Most observed deformation patterns observed are ordered in space and with time, and their types depend on the plastic flow law. It is shown that the $V_{aw} \sim (\theta)^{-1}$ dependence is valid for the linear work hardening stage alone, i.e. for ???, which agrees with data acquired on Cu single crystals [20]. The localized plasticity picture for the parabolic work hardening stage consists of stationary zones and would remain unaltered.

A similar behavior is reported by other researchers, e.g., Roth who has also obtained a parabolic loading diagram [21].

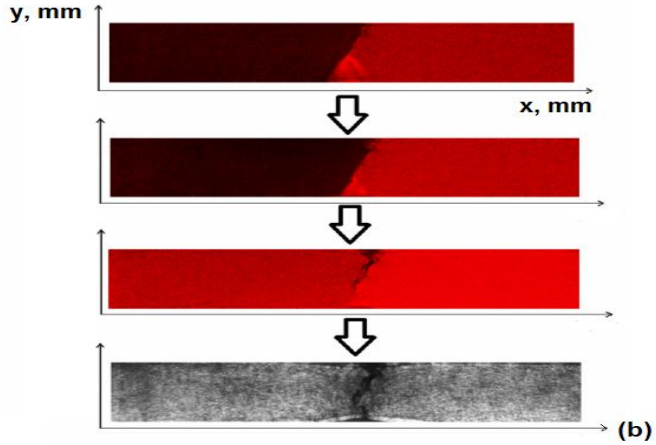

Fig. 5: Pictures of localized zones evolution during pre-fracture stages at a deformation ε_{tot} =0.32 ÷ 0.335 for (a) initial bimetal and (b) after 6 h of electrolytic hydrogenation.

The propagation velocity V_{aw} and spatial period λ of plastic deformation localization zones for bimetal are given in Table 2 together with values for stainless and low-carbon steels [10]. A satisfactory agreement with the all-purpose inversely proportional relation between the macrolocalized plastic-strain autowave velocity and the θ work-hardening coefficient normalized by the shear modulus of the material [9, 20] is evident. The profile of this dependence ($V_{aw} \sim 1/\theta$) deviates from the well-known plasticity Kolsky waves described by the law $V_{pl} \sim \sqrt{\theta}$. The distinction between the above two dependences enables one to conclude that using the one digital image correlation method enabled for a discovery of a novel type of wave processes upon the uniaxial tension, presented by self-excited waves of plastic flow. The localized plasticity picture monitored for the parabolic work hardening stage comprises stationary zones and would remain unaltered. The identical case was described in [21].

Table 2: Propagation velocity V_{aw} and spatial period λ of plastic deformation localization zones

Material	λ (mm)	$V_{aw} \cdot 10^5$ (m/s)
Stainless steel [10]	4.0	3.5
Low-carbon steel [10]	8.0	5.3
Bimetal	4.0	6.0

Afore observed complex deformation of the bimetal allows one to assume that the emergence of a single localized maximum is a manifestation of noticeably altered material properties. This is indirectly pronounced, for example, by the occurrence of an extremum in the ultrasound rate plotted versus deformation a short time before necking is initiated in tensile metals and alloys. Through the flow localization patterns, one can monitor the jumpwise changes in plasticity of alloys shell at the onset of the rolling, which is undetectable by other tools. In order to keep unchanged the uniform ductility over the bulk of the material, dies and mandrel profiles should be properly chosen, else the reduction mode might be changed (see, e.g. [9, 10]).

4. Conclusions

Deformation peculiarities of the bimetal exposed to high-temperature tempering and saturated with hydrogen in a three-electrode electrochemical cell at a controlled constant cathode potential for 6 hours were studied. The mechanical properties of the bimetal were established in the two states. The characterization of stainless steel - low-carbon steel composite upon the uniaxial tension enabled one to highlight the following deformation specifities of plastic bimetals. Localized plastic deformation zones formed and evolved during the plastic flow in a basic metal. The cladding layer in the material prevented the Lüders bands propagation with a constant velocity from the machine clamp serving as a basic stress concentrator. The emerged bands moved abruptly with other Lüders bands from the cladding metal - basic metal inner interfaces and past through the whole cross-section of specimen. Fragmentation and destruction of the bimetal were caused by stress concentrators arisen at the cladding metal - basic metal inner interface.

The localization behavior of plastic deformation is the most pronounced feature of bimetal. Through a constant-rate tensile loading, space-time periodic structures, called patterns, emerge in a strained sample from the yield limit to its failure. Four localized plasticity patterns were observed empirically for all studied materials with different chemical and phase compositions, crystal lattice types (FCC, BCC or HCP), grain sizes and deformation mechanisms.

A comparison of data prior to and after hydrogenation of bimetal revealed that hydrogen enhanced the plastic deformation localization. In contradistinction to a pristine material, hydrogenized samples exhibited more ductile fraction, indicating that hydrogen at-

oms increased plasticity of the austenitic stainless steel layer in a test bimetal.

Acknowledgement

This work was supported within the Fundamental Research Program of the State Academies of Sciences for 2017–2020; the Tomsk State University Competitiveness Improvement programme and the Russian Foundation for Basic Research (project no. №16-08-00385-a.)

References

[1] M. Acarer, B. Gulenc, F. Findik (2003), Investigationm of explosive welding. parameters and their effects on microhardness. *Materials & Design* 24, 659-664.
[2] N. Venkateswara, G. Madhusudhan, S. Nagarjuna (2011), Weld overlay cladding of high strength low alloy steel with austenitic stainless steel–structure and properties. *Materials & Design* 32, 2496-2506.
[3] F. Findik, R. Yilmaz, T. Somyurek (2011), The effect of heat treatment on the microstructure and microhardness of explosive welding. *Scientific Research and Essays*. 6, 4141-4151.
[4] L. Guobin, W. Jianjun, L. Xiangzhi, L. Guiyun (1998), The properties and application of bimetal hot-forging die. *Journal of Materials Processing Technology.* 75, 152-156.
[5] L. Mehnen, H. Pfutzner, E. Kaniusas (2000), Magnetostrictive amorphous. bimetal sensors. *Journal of Magnetism and Magnetic Materials.* 215, 779-781.
[6] J. Nakano, Y. Miwa, T. Tsukada, M. Kikuchi, S. Kita, Y. Nemoto, H. Tsuji, S. Jitsukawa (2002), Characterization of 316L(N)-IG SS joint produced by hot isostatic pressing technique. *Journal of Nuclear Materials.* 307, 1568-1572.
[7] H.R. Akramifarid, H. Mirzadeh, M.H. Parsa (2014), Cladding of aluminum on AISI 304L stainless steels by cold roll bonding: mechanism, microstructure, and mechanical properties. *Materials Science and Engineering*. 613, 232-239.
[8] S.A. Barannikova (2000), Localization of stretching strain in doped carbon gamma-Fe single crystals. *Technical Physics.* 45, 1368-1370.
[9] L.B. Zuev, V.I. Danilov, S.A. Barannikova, I.Y. Zykov (2000), A new type of plastic deformation waves in solids. *Journal of Applied Physics.* A 71, 91-94.
[10] L.B. Zuev, S.A. Barannikova (2011), Plastic flow localization viewed as auto-wave process generated in deforming metals. *Solid State Phenomena.* 172-174, 1279-1283.
[11] V.P. Ramunni, T. De Paiva Coelho, P.E.V. de Miranda (2006), Interaction of hydrogen with the microstructure of low-carbon steel. *Materials Science and Engineering.* 435–436, 504–514.
[12] H. Fuchigami,. H. Minami, M. Nagumo (2006), Effect of grain size on the susceptibility of martensitic steel to hydrogen-related failure. *Philosophical Magazine Letters.* 86, 21–29.
[13] Y. Kim,. Yu. Kim, D. Kim, S. Kim, W. Nam, H. Choe (2011), Effects of hydrogen diffusion on the mechanical properties of austenite 316L steel at ambient temperature. *Materials Transactions*. 52, 507 – 513.
[14] G.T. Park, S.U. Koh, H.G. Jung, K.Y. Kim (2008), Effect of microstructure on the hydrogen rapping efficiency and hydrogen induced cracking of pipeline steel. *Corrosion Science.* 1865-1871
[15] L. Chen, Z. Yang, B. Jha, G. Xia, J.W. Stevenson (2005), Clad metals, roll bonding and their applications for SOFC interconnects. *Journal of Power Sources.* 152, 40-45.
[16] S.A. Barannikova, A.G. Lunev, M.V. Nadezhkin, L.B. Zuev (2014), Effect of hydrogen on plastic strain localization of construction steels. *Advanced Materials Research.* 880, 42-47.
[17] S. Sozen (2015), Determination of displacement distributions in welded steel tension elements using digital image techniques. *Steel and Composite Structures.* 18, 1103-1117.
[18] D. Sokoli, W. Shekarchi, E. Buenrostro, M. Wassim (2014), High-strength reinforcement in columns under high shear stress, *Earthquake engineering.* 7, 609-626.
[19] L.B. Zuev, V.V. Gorbatenko, S.N. Polyakov (2002), Instrumentation for speckle interferometry and techniques for investigation deformation and fracture. *Proceedings of SPIE.* 4900, 1197.
[20] A. Acharya, A. Beaudoin, R. Miller (2008), New perspectives in plasticity theory. Dislocation Nu- cleation, waves, and partial continuity of plastic strain rate. *Mathematics and Mechanics of Solids*. 13, 292 -315.
[21] A. Roth, T.A. Lebedkina, M.A. Lebyodkin (2012), On the critical strain for the onset of plastic instability in an austenitic FeMnC steel. *Materials Science and Engineering.* 539, 280-284.